Deep learning: step forward to high-resolution in vivo shortwave infrared imaging

Vladimir A Baulin, Yves Usson, Xavier Le Guével

Deep learning image analysis for *in vivo* shortwave infrared imaging

Vladimir A. Baulin,[1,*] Yves Usson,[2] and Xavier Le Guével[3]

[1] *Departament Química Física i Inorgànica, Universitat Rovira i Virgili, Marcel.lí Domingo s/n, 43007 Tarragona, Spain*

[2] *TIMC-IMAG Laboratory, University of Grenoble Alpes, CNRS-UMR 5525, 38700 Grenoble, France*

[3] *Cancer Targets and Experimental Therapeutics, Institute for Advanced Biosciences (IAB), University of Grenoble Alpes (UGA)/ INSERM-U1209/ CNRS-UMR 5309, 38700 Grenoble, France*

(Dated: February 16, 2021)

In vivo optical imaging in the shortwave infrared windows (1000-1700 nm) has shown a growing interest with major improvement in terms of spatial and temporal resolution in depth down to 4 mm compared to the NIR-I region (700-900 nm). This method can be particularly useful for studies of the growth and development of blood vessels in tumors, in vivo monitoring of pathologies and evaluation of effects of drugs. SWIR signal obtained from vessels passes through tissues and skin and thus, subject to noise and scattering. We demonstrate that the combination of SWIR imaging in the NIR-IIb (1500-1700 nm) region with advanced deep learning image analysis on small animals can provide a non-intrusive deep insight into the morphology of the blood vessels. For demonstration we use neural network IterNet that exploits structural redundancy of the blood vessels (L. Li, et.al., The IEEE WACV, 2020). It can reconstruct the blood vessels structure in high details, thus providing a useful analysis tool for raw SWIR images.

Keywords: deep learning, microvessels, SWIR, fluorescence

I. INTRODUCTION

The field of *in vivo* optical imaging for biomedical applications is growing rapidly over the last two decades leading to more precise diagnostic of early stage diseases and to advanced image-guided-surgery system already available in clinics (10.3389/fbioe.2019.00487). One of these breakthroughs is related to the development of innovative imaging systems in the shortwave infrared (SWIR) spectral window, called also NIR-II, between 900 and 1700 nm. SWIR has demonstrated a major improvement in terms of spatial and temporal resolution, reaching deep in tissue up to 4 to 6 mm compared to the Visual light (400-700 nm) and NIR-I (700-900 nm) regions. The benefit moving forward from NIR-I to SWIR has mainly been associated to the weak auto-fluorescence and reduced scattering from the living tissues at longer wavelengths.[1] For instance, it was shown recently the striking improvement of detection with higher signal-to-noise ratio selecting the SWIR sub-windows NIR-IIb (1500-1700 nm) for *in vivo* imaging.[2–4] The concomitant progress of the sensor detection in the SWIR range and of the formulation of new bright and biocompatible SWIR emitting organic and inorganic contrast agents[5–8] has enabled to use these optical systems for intra-operative surgery in small animals[9,10] and recently in human.[11] One of the most appealing field of applications for SWIR imaging concerns the (micro)vascularization, where SWIR imaging allowing to monitor in real time non-invasively different pathologies such as vascular disorders, (neo)angegiogenosis in cancer, wound healing, implants.[6,12–14]

Despite these major steps, we are still far to reach the spatial resolution at high depth achieved by X-ray imaging.[15] Others recent optical imagings based on full field optical coherence (10.1364/BOE.9.000557) and high-resolution optoacoustic imaging (10.1039/C6CS00765A) can lead to spatial resolution down to 1.7um but with a quite short limit of view that requires long time acquisition to image the whole animal. A promising strategy to overcome this issue relies on the imaging treatment of SWIR images by iterative treatment. It will enable to isolate the (micro)vessels, to reduce scattering light originated from the tissue, and detect 3D blood vessels structures in order to provide a full structural analyses. We recently demonstrated the significant improvement of contrast and spatial resolution in mice using Monte Carlo Restoration which enabled to perform segmentation analysis of small animal presenting vascular disorder.[16] Herein, we propose to use deep learning based on IterNet network on SWIR NIR-IIb imaging to demonstrate the high potential of this method to go

one-step further to high-resolution optical imaging that could be easily transferred in clinics and hospitals.

II. EXPLOITING STRUCTURAL REDUNDANCY IN SWIR IMAGES

Deep Neural Network IterNet[17] is based on a popular neural network U-Net,[18] a fully connected convolutional neural network that uses strong data augmentation allowing to reduce significantly the number of training images. IterNet goes further and uses structural redundancy or self-similarity of blood vessels that allows the network to find obscured details of the vessel from the segmented vessel image itself, rather than the raw input image. As a result, IterNet can learn from 10–20 annotated images (ground truth) to provide a good accuracy.

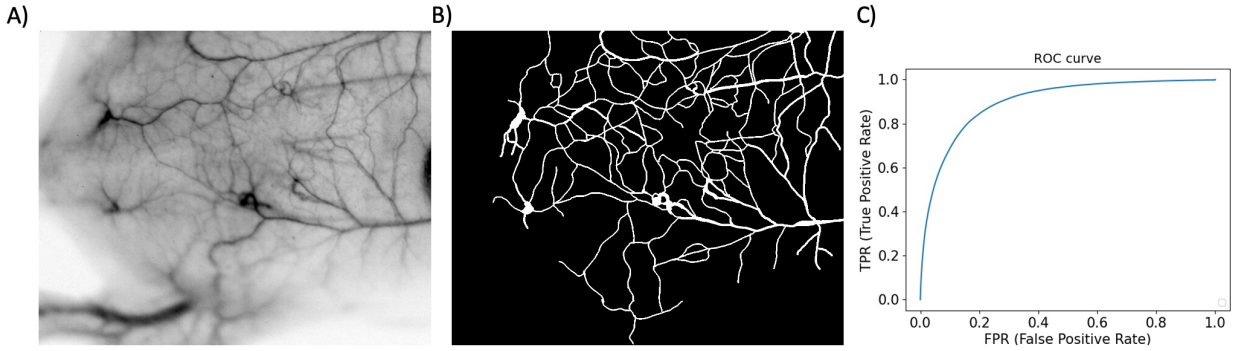

FIG. 1. a) Original SWIR image used for training; b) annotation of ground truth; c) Resulting receiver operating characteristic (ROC) curve of the performance of the training on SWIR images. Area under the curve: 0.90; Area under precision-recall curve: 0.57, Jaccard similarity score: 0.89

IterNet is proven to be number one in ratings for performance in segmentation of blood vessels. The performance is tested on open databases of blood vessels in retina vessels on three mainstream datasets, DRIVE, CHASE_DB1, STARE, which are used as as a gold standard for performance benchmarking and comparison for blood vessels segmentation methods. It has a high accuracy measured in AUCs of 0.9816, 0.9851, and 0.9881 for DRIVE, CHASE_DB1, and STARE, respectively, which is the best result at the moment.

A specially trained neural network on manually annotated black and white images

Parameters used: batch_size=32, repeat=10, minimum_kernel=32, epochs=200, itera-

tion=3, crop_size=128, stride_size=3

Original probability weights of IterNet neural network trained on images from open databases DRIVE, CHASE-DB1, and STARE were used for comparison of performance.

III. SWIR IMAGES ACQUISITION

SWIR imaging was performed using a Princeton camera 640ST (900-1700 nm) coupled with a laser excitation source at L = 808 nm (100 mW/cm^2). We use short-pass excitation filter at 1000 nm (Thorlabs) and long-pass filter on the SWIR camera from Thorlabs (LP1500 nm). 25 mm or 50 mm lenses with numerical aperture (n.a) = 1.4 (Navitar) were used to focus on the mice. 25 mm and 50 mm lenses provide a theoretical spatial resolution of 400 microns and 150 microns respectively. NMRI nude mice (Janvier, France) were anesthetized (air/isofluorane 4% for induction and 1.5% thereafter) and were injected intravenously via the tail vein (200 µL of Indocyanine Green (ICG) at 500 µM in PBS). *In vivo* SWIR imaging were performed using 25 mm or 50 mm lenses and LP1500 nm at different exposure times (100 ms to 1 s). For the *ex vivo* images of the inner skin, the mice skin flap of 2 to 3 mm thick were soaked in formaldehyde just after sacrificed. Images were taken on the inner side of the flap with an Andor camera under white light illumination (zoom x0.8; 1 s exposure).

IV. BLOOD VESSELS MORPHOLOGY

A. Neural network prediction

(junctions, overlap, 3D shape)

B. Validation of the morphology

Fig. 2A is the image of the mouse made with the SWIR camera with the 25 mm lens under the white light (from a neon which has a broad excitation) before injection of contrast agent and long time exposure. The image on the left after injection of the contrast agent (ICG) using a 808 nm excitation (100 mW/cm^2) at 100 ms exposure. The SWIR detection allows a very good transparency of the skin with weak auto-fluorescence and scattering on the first few mm. Therefore we can see nicely the blood vessels

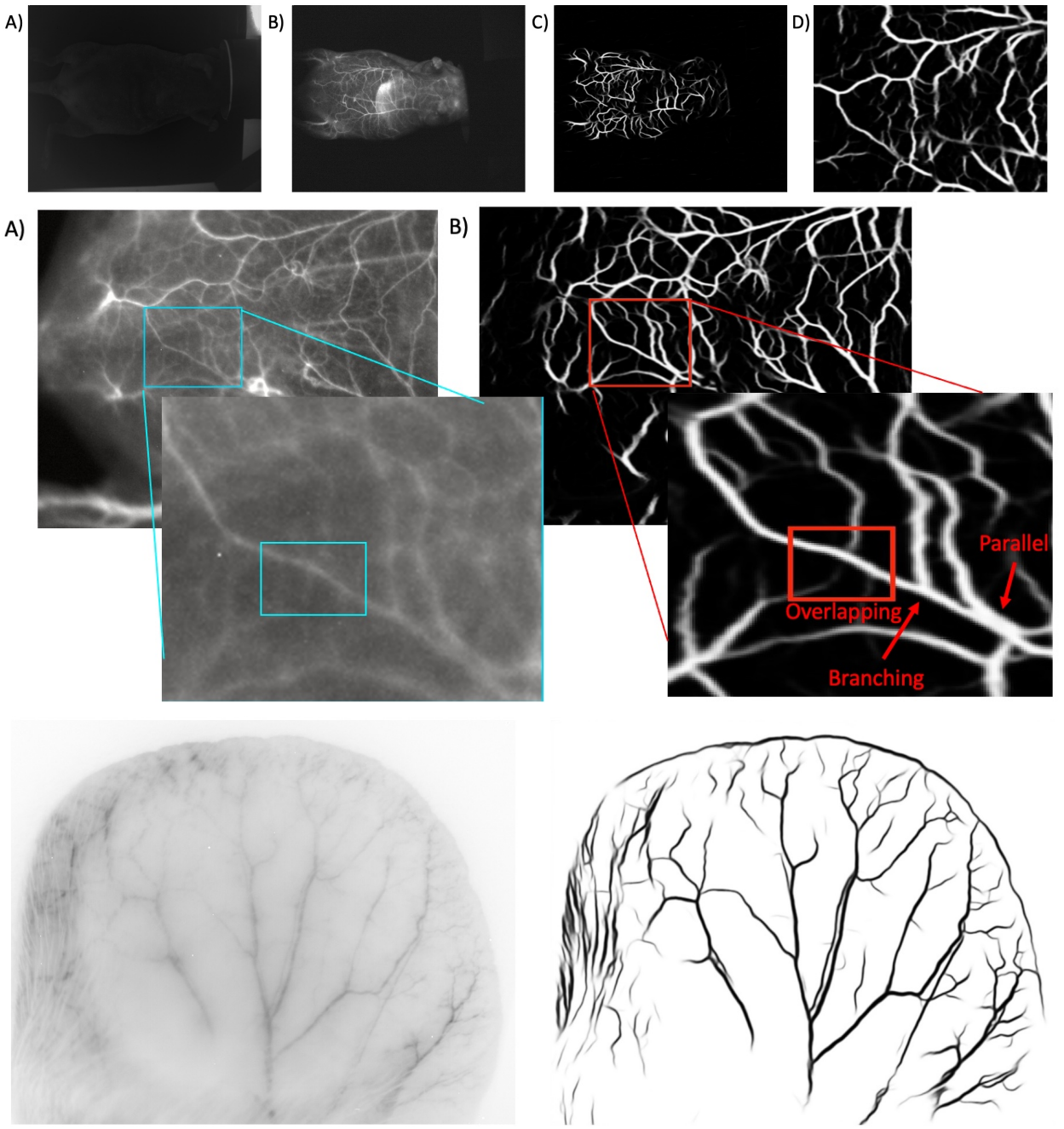

FIG. 2. A) Original SWIR image with a detail in the inset; B) Segmented image with a detail in the inset.

V. BLOOD VESSELS ANALYSIS

(artery and veins, marker propagation, skeletonization)

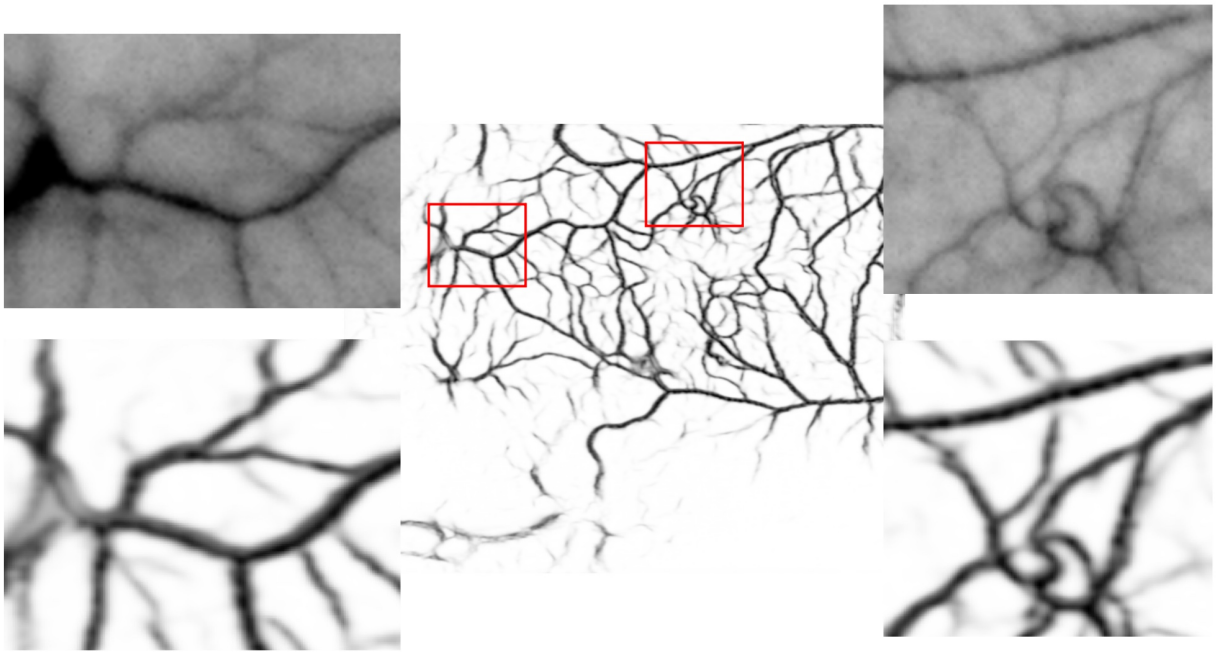

FIG. 3. A) A fragment of the original SWIR image showing complex topology of the blood vessel network. B) Predicted blood vessel structure showing junctions and cross-sections of the vessels.

VI. CONCLUSIONS

NN enable to :1) see vessels overlap and junction, 2) obtain kind of morphology with a 3D shape of blood vessels, 3) improve contrast enough to see clearly artery to vein in the ear mice, 5) obtain more accurate kinetic of blood flow

ACKNOWLEDGMENTS

XLG would like to thanks Maxime Henry and Benjamin Musnier for the animal experiments and Plan cancer (C18038CS) for their financial support. The Optimal imaging platform is supported by France Life Imaging (French program “Investissement d’Avenir” grant; “Infrastructure d’avenir en Biologie Santé”, ANR-11-INBS-0006) and the IBISA French consortium “Infrastructures en Biologie Santé et Agronomie”.

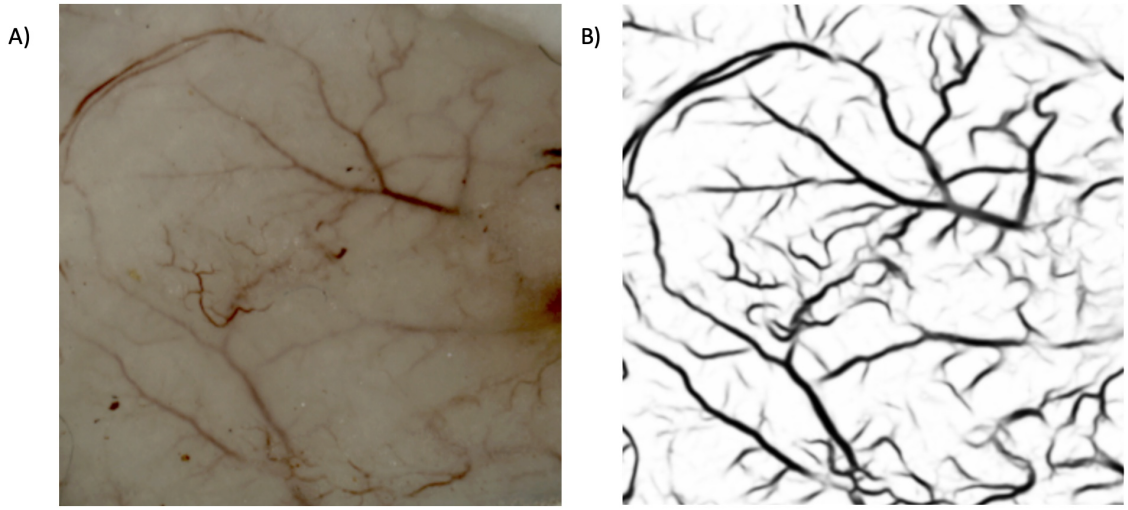

FIG. 4. A) Fragment of the original SWIR image; B) Overlay of predicted vessel structure and original image. Arteries (red) and veins (blue) made by SeqNet network.; C) Prediction of arteries (red) and veins (blue) made by SeqNet network.

SUPPLEMENTARY INFORMATION

Analysis of the SWIR video with deep learning and skeletonization algorithms.

---

* vladimir.baulin@urv.cat

[1] G. Hong, A. L. Antaris, and H. Dai, Nat Biomed Eng **1**, 0010 (2017).

[2] Y. Zhong, Z. Ma, F. Wang, X. Wang, Y. Yang, Y. Liu, X. Zhao, J. Li, H. Du, M. Zhang, Q. Cui, S. Zhu, Q. Sun, H. Wan, Y. Tian, Q. Liu, W. Wang, K. C. Garcia, and H. Dai, Nat Biotechnol **37**, 1322 (2019).

[3] K. Wang, Q. Wang, Q. Luo, and X. Yang, Opt. Express **23**, 12669 (2015).

[4] B. Musnier, M. Henry, J. Vollaire, J. Coll, Y. Usson, V. Josserand, and X. Le Guével, J. Biophotonics (2020), 10.1002/jbio.202000345.

[5] C. Li, G. Chen, Y. Zhang, F. Wu, and Q. Wang, J. Am. Chem. Soc. **142**, 14789 (2020).

[6] S. Zhu, R. Tian, A. L. Antaris, X. Chen, and H. Dai, Adv. Mater. , 1900321 (2019).

[7] B. Musnier, K. D. Wegner, C. Comby-Zerbino, V. Trouillet, M. Jourdan, I. Häusler, R. Antoine, J.-L. Coll, U. Resch-Genger, and X. Le Guével, Nanoscale **11**, 12092 (2019).

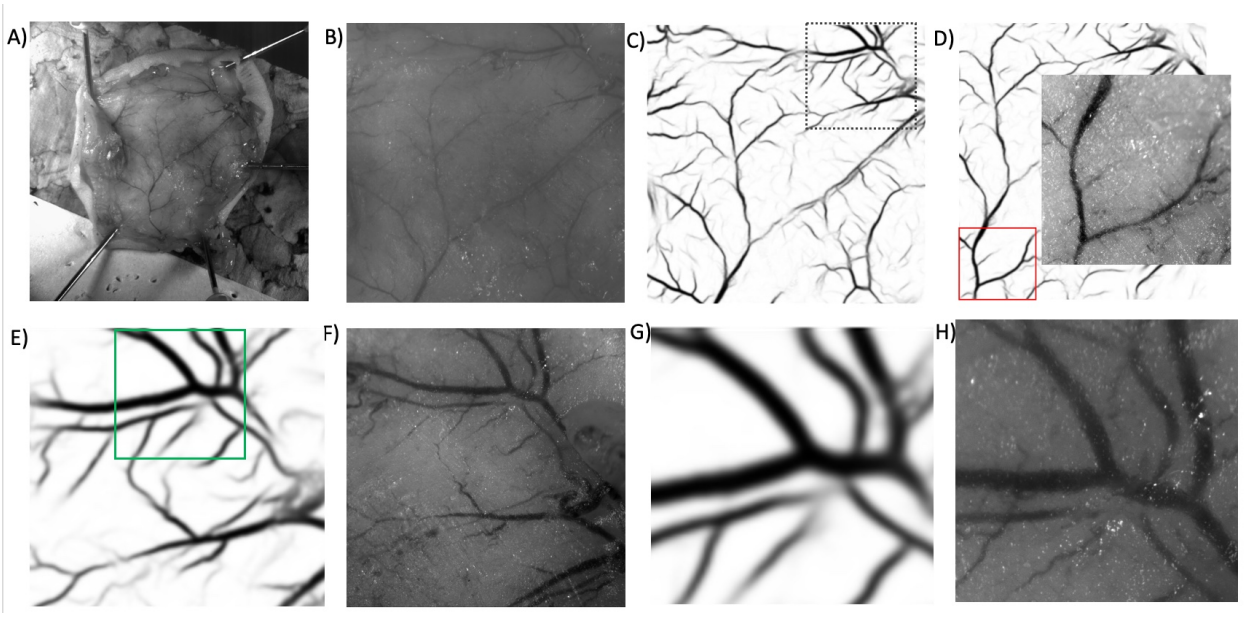

FIG. 5. A) Fragment of the original SWIR image; B) Overlay of predicted vessel structure and original image. Arteries (red) and veins (blue) made by SeqNet network; C) Prediction of arteries (red) and veins (blue) made by SeqNet network.

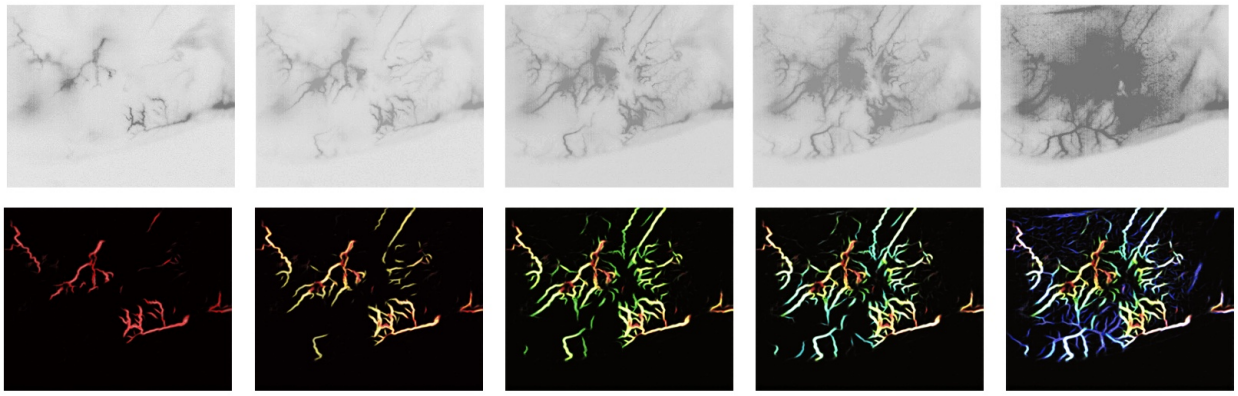

FIG. 6. A) Original SWIR image in a sequence of first frames where the fluorescent marker propagates through the blood network. B) Combined inferrence image (sum of predicted images from individual frames).

[8] S. Wang, B. Li, and F. Zhang, ACS Cent. Sci. **6**, 1302 (2020).

[9] S. Zhu, Z. Hu, R. Tian, B. C. Yung, Q. Yang, S. Zhao, D. O. Kiesewetter, G. Niu, H. Sun, A. L. Antaris, and X. Chen, Adv. Mater. **30**, 1802546 (2018).

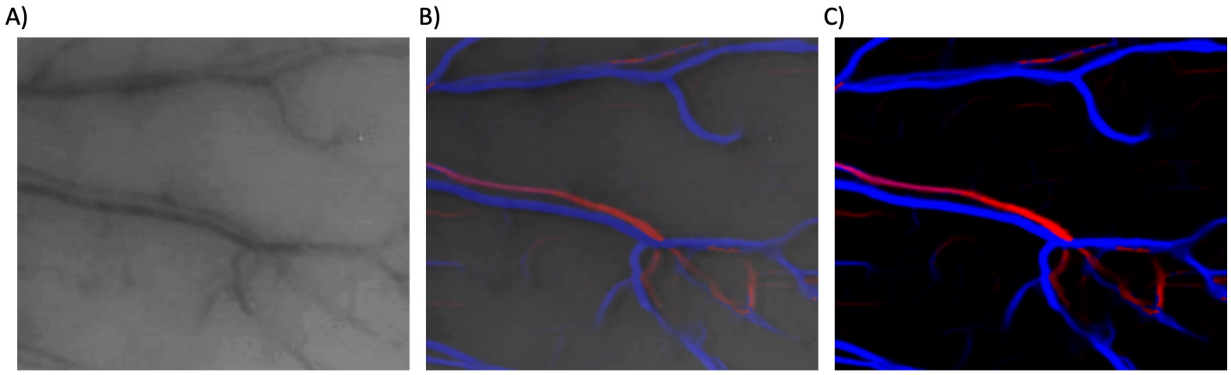

FIG. 7. A) Fragment of the original SWIR image; B) Overlay of predicted vessel structure and original image. Arteries (red) and veins (blue) made by SeqNet network; C) Prediction of arteries (red) and veins (blue) made by SeqNet network.

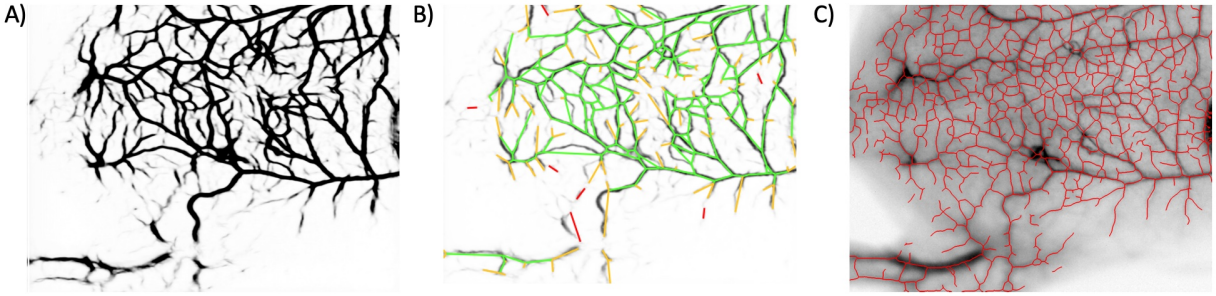

FIG. 8. Skeletonization of the inferred image.

[10] J. Du, S. Liu, P. Zhang, H. Liu, Y. Li, W. He, C. Li, J. H. C. Chau, R. T. K. Kwok, J. W. Y. Lam, L. Cai, Y. Huang, W. Zhang, J. Hou, and B. Z. Tang, ACS Appl. Mater. Interfaces **12**, 8040 (2020).

[11] Z. Hu, C. Fang, B. Li, Z. Zhang, C. Cao, M. Cai, S. Su, X. Sun, X. Shi, C. Li, T. Zhou, Y. Zhang, C. Chi, P. He, X. Xia, Y. Chen, S. S. Gambhir, Z. Cheng, and J. Tian, Nat Biomed Eng **4**, 259 (2020).

[12] M. Saif, W. J. Kwanten, J. A. Carr, I. X. Chen, J. M. Posada, A. Srivastava, J. Zhang, Y. Zheng, M. Pinter, S. Chatterjee, S. Softic, C. R. Kahn, K. van Leyen, O. T. Bruns, R. K. Jain, and M. G. Bawendi, Nat Biomed Eng **4**, 801 (2020).

[13] F. Wang, H. Wan, Z. Ma, Y. Zhong, Q. Sun, Y. Tian, L. Qu, H. Du, M. Zhang, L. Li, H. Ma, J. Luo, Y. Liang, W. J. Li, G. Hong, L. Liu, and H. Dai, Nat Methods **16**, 545 (2019).

[14] Z. Ma, M. Zhang, J. Yue, C. Alcazar, Y. Zhong, T. C. Doyle, H. Dai, and N. F. Huang, Adv. Funct. Mater. **28**, 1803417 (2018).

[15] F. Wang, P. Zhou, K. Li, M. Mamtilahun, Y. Tang, G. Du, B. Deng, H. Xie, G. Yang, and T. Xiao, IUCrJ **7**, 793 (2020).

[16] Z. Yu, B. Musnier, K. D. Wegner, M. Henry, B. Chovelon, A. Desroches-Castan, A. Fertin, U. Resch-Genger, S. Bailly, J.-L. Coll, Y. Usson, V. Josserand, and X. Le Guével, ACS Nano **14**, 4973 (2020).

[17] L. Li, M. Verma, Y. Nakashima, H. Nagahara, and R. Kawasaki, in *The IEEE Winter Conference on Applications of Computer Vision (WACV)* (2020).

[18] O. Ronneberger, P. Fischer, and T. Brox, arXiv:1505.04597 [cs] (2015), arXiv: 1505.04597.